Numerical Simulation of Cavitating Flows on a Foil by Using Bubble Size Distribution Model

Yutaka ITO, Takao NAGASAKI
Tokyo Institute of Technology
4259 Nagatsuta-cho, Midori-ku, Yokohama, 226-8502, JAPAN
ito@es.titech.ac.jp

Keywords: Simulation, Cavitation, Foil, Bubble size distribution model

Abstract

A new cavitating model by using bubble size distribution based on bubbles-mass has been proposed. Both liquid and vapor phases are treated with Eulerian framework as a mixture containing minute cavitating bubbles. In addition vapor phase consists of various sizes of vapor bubbles, which are distributed to classes based on their mass. The bubble number-density for each class was solved by considering the change of the bubble-mass due to phase change as well as generation of new bubbles due to heterogeneous nucleation. In this method, the bubble-mass is treated as an independent variable, and the other dependent variables are solved in spatial coordinates and bubble-mass coordinate.

Firstly, we employed this method to calculate bubble nucleation and growth in stationary super-heated liquid nitrogen, and bubble collapse in stationary sub-cooled one. In the case of bubble growth in super-heated liquid, bubble number-density of the smallest class based on its mass is increased due to the nucleation. These new bubbles grow with time, and the bubbles shift to larger class. Therefore void fraction of each class is increased due to the growth in the whole class. On the other hand, in the case of bubble collapse in sub-cooled liquid, the existing bubbles are contracted, and then they shift to smaller class. It finally becomes extinct at the smallest one.

Secondly, the present method is applied to a cavitating flow around NACA0015 foil. Liquid nitrogen and liquid oxygen are employed as working fluids. Cavitation number, σ, is fixed at 0.15, inlet velocities are changed at 5, 10, 20 and 50m/s. Inlet temperatures are 90K in case of liquid nitrogen, and 90K and 110K in case of liquid oxygen. 110K of oxygen is corresponding to the 90K of nitrogen because of the same relative temperature to the critical one, $T_r=T/T_c$. Cavitating flow around the NACA0015 foils was properly analyzed by using bubble size distribution.

Finally, the method is applied to a cavitating flow in an inducer of the LE-7A hydrogen turbo-pump. This inducer has 3 spiral foils. However, for simplicity, 2D calculation was carried out in an unrolled channel at 0.9R cross-section. The channel moves against the fluid at a peripheral velocity corresponding to the inducer revolutions. Total inlet pressure, Pt_{in}, is set at 100KPa, because cavitation is not generated at a design point, Pt_{in}=260KPa. The bubbles occur upstream of the foils and collapse between them. Cavitating flow in the inducer was successfully predicted by using the bubble size distribution.

Introduction

Cavitation in turbo-pumps is one of the important problems in developing a liquid fuel rocket engine. At present technology, it is difficult to predict the cavitation and its influence on the performance of turbo-pumps accurately. Especially cryogenic cavitation is complex because cryogenic fluids, such as LH_2, LOX and LN_2, have smaller latent heat and lower temperature level than ordinary fluids like H_2O, and they easily boils by heat influx from the surroundings. The development of reliable and efficient numerical code for a high-speed cryogenic cavitating flow is strongly desirable in order to predict the performance at a design stage and reduce number of prototypes or experiments.

The authors developed a strict numerical code [1] for a high-speed cryogenic cavitating flow. It employed a model that has the following two features; 1: A compressible liquid phase was dealt with Eulerian framework as a mixture containing minute cavitating bubbles. 2: Cavitating bubbles were treated with Lagrangian approach, in other words, each bubble was distinguished and traced. The results showed good agreement with NASA experimental data [2] by Simoneau & Hendricks. It needed, however, large memory and CPU power in proportion to the volume of calculation domain, independent of number of numerical grids, because all of the bubbles were distinguished and traced. Such a direct simulation of each bubble is possible for a small flow-field like a Laval nozzle, but it is difficult to handle a large flow-field such as the turbo-pumps of the rocket.

Tani et al. [3] and Schnerr et al. [4] treated the cavitating flow-field as a mixture and obtained good results. However, they took no thought of bubble size distribution in a control volume. When we analyze a rotating cavitation in the turbo-pumps for example, it is supposed that analysis for the flow-field in which both tiny and large bubbles exist together will become important.

In this study, consequently, a new model is proposed to deal with the bubble size distribution. The liquid model is the same as the previous one. Vapor phase consists of various sizes of minute vapor bubbles, which is distributed to classes based on their mass. The change of bubble number density for each class was solved by considering the change of bubble-

mass due to phase change as well as generation of new bubbles due to heterogeneous nucleation. In this method the bubble-mass is treated as an independent variable, in other word, a new coordinate, and dependant variables are solved in Eulerian framework for spatial coordinates and bubble-mass coordinate. The present model can deal with the bubble size distribution with much less computational effort than the Lagrangian simulation of each bubble.

Nomenclature

Cp	pressure coefficient
e	total energy
$\mathbf{F_D}$	friction vector
h	enthalpy
Ma	Mach number
m_0	mass of one molecule
N	probability function of bubble number-density
n	bubble number-density
n_0	number of "seeding nuclei" per unit volume
$\dot{n}$	nucleation rate
P	pressure
R	radius
r	distance from the center of rotational system
T	temperature
t	time
$\mathbf{V}$	velocity vector
w	mass of a bubble
α	volume fraction occupied in a control volume
β	coefficient of apparent mass
Γ	rate of phase change per a bubble
δ	delta function
Λ	mass of nucleation rate per unit volume
λ	thermal conductivity
μ	viscosity
π	circulation ratio
ρ	density
σ	coefficient of surface tension
ϕ	parameter of contact angle on the "seeding nuclei
ω	angular velocity vector
index	
G	vapor
in	inlet
L	liquid
S	slip between liquid and bubbles
sat	saturation
0	nucleation

Mixture model

For the Eulerian framework of the liquid phase, the flow field is divided into control volumes, each filled up with the mixture containing minute vapor bubbles. Generally it is well known that pure liquid behaves like incompressible fluid whose average sound speed is large, however, liquid containing bubbles behaves as compressible fluid whose average sound speed is small. Based on void fraction in the control volume, the average sound speed is, therefore, calculated, so the effect of containing bubbles is taken into account. Besides, since compressibility of the pure liquid is considered, sub-cooled condition can be rigorously calculated. By using this model, basic equations for the liquid phase are given as followings.

Mass conservation equation

$$\frac{\partial}{\partial t}(\alpha_L\rho_L)+\nabla(\alpha_L\rho_L\mathbf{V}_L)=-\Lambda_G-\int_0^\infty(N\Gamma_G)dw \tag{1}$$

where,

$$\Lambda_G=\frac{4\pi}{3}R_0^3\rho_G\dot{n} \tag{2}$$

$$\Gamma_G=\frac{d}{dt}\left(\frac{4\pi}{3}R_0^3\rho_G\right) \tag{3}$$

Momentum equation

$$\begin{aligned}&\frac{\partial}{\partial t}(\alpha_L\rho_L\mathbf{V}_\mathbf{L})+\nabla(\alpha_L\rho_L\mathbf{V}_\mathbf{L}\mathbf{V}_\mathbf{L})\\&=\alpha_L\nabla P+\alpha_L\mu_L\Delta\mathbf{V}_\mathbf{L}-\Lambda_i\mathbf{V}_\mathbf{L}-\int_0\{N\Gamma_G\}dw\mathbf{V}_\mathbf{L}\\&\quad-\int_0(N\mathbf{F_D})dw+\alpha_l\rho_l\{\omega\times\mathbf{V}_\mathbf{L}+\omega\times(\omega\times\mathbf{r})\}\end{aligned} \tag{4}$$

Energy equation

$$\begin{aligned}&\frac{\partial}{\partial t}(\alpha_L\rho_Le_L)+\nabla(\alpha_L\rho_Le_L\mathbf{V}_\mathbf{L})+\alpha_L\nabla(p\mathbf{V}_\mathbf{L})\\&=-\Lambda_Gh_G-\int_0(N\Gamma_Gh_G)dw\end{aligned} \tag{5}$$

Bubble size distribution model

The vapor phase in targeted flow fields consists of minute bubbles ranging from sub-micrometer to sub-millimeter. Therefore the bubbles are assumed to be a cloud of spherical bubbles, and all bubbles are filled with saturated vapor. In the control volume there are bubbles with various size. Therefore, a coordinate of bubble-mass (w) is defined in addition to the spatial coordinates (x, y, z). A distribution of probability of bubble number-density, N, is shown in Fig. 1, for example. N is treated with Eulerian framework with respect to x, y, z and w. By using this model, basic equations for the vapor phase are written as followings.

Number density of bubbles

$$n=\int Ndw \tag{6}$$

Mass of bubbles

$$m_G=\int\left(\frac{4\pi}{3}R^3\rho_GN\right)dw=\int(wN)dw \tag{7}$$

Conservational equation of probability function of bubble number-density

$$\frac{\partial}{\partial t}N+\nabla(N\mathbf{V_G})+\frac{\partial}{\partial w}(N\Gamma_G)=\dot{n}\delta(w-w_0) \tag{8}$$

where, $\dot{n}$ is nucleation rate based on the heterogeneous nucleation theory mentioned below.

Translational momentum equation of bubbles

$$\beta\frac{4\pi}{3}R^3\rho_L\left(\frac{\partial}{\partial t}\mathbf{V_S}+\mathbf{V_G}\nabla\mathbf{V_G}+\mathbf{V_L}\nabla\mathbf{V_L}\right) \quad (9)$$

$$=\mathbf{F_D}-\frac{4\pi}{3}R^3\nabla P$$

where,

$$\mathbf{V_S}=\mathbf{V_G}-\mathbf{V_L} \quad (10)$$

$$\mathbf{F_D}=-C_D\pi R^2\rho_L\frac{|\mathbf{V_S}|\mathbf{V_S}}{2} \quad (11)$$

Volume fraction

$$\alpha_G=\int_0^\infty\left(N\frac{4\pi}{3}R^3\right)dw \quad (12)$$

$$\alpha_L+\alpha_G=1 \quad (13)$$

According to these relations, the bubbles are distributed to the classes based on their mass. Each class has n, m_G, Γ_G and u_G. In addition, the smallest class has Λ_G.

The expansion or contraction rate of the vapor bubble, dR/dt, is dominated by two mechanisms; a momentum that is needed to push away or pull up ambient liquid, and a heat transfer that is needed to drive phase change at the interface between the bubble and ambient liquid. They are called the inertia (momentum) control and the heat transfer control, respectively. Generally speaking, in the expansion process the bubble radial movement is dominated by the inertia only at first and then changes to the heat transfer control. Over the whole contraction process it is controlled by the inertia [5]. Therefore, for simplicity, effects of both heat transfer and inertia are considered in case that bubble size is less than 1μm, but an effect of heat transfer only is considered in case that bubble size is larger than 1μm. Details of the dR/dt calculation are shown in reference (6).

Numerical method

Figure 2 shows a flowchart of a calculation procedure. In the advection stage, SHUS (Simple High-resolution Upwind Scheme) approach [7] with 3rd order MUSCL (Monotonic Upwind-centered Scheme for Conservation Laws) interpolation [8] is applied to the spatial integration. In the bubble movement stage, a slip velocity between the liquid and the bubbles of each class is calculated. A friction force between them is also taken into account. In the time marching of unsteady analysis, four-stage 2nd order Runge-Kutta scheme is employed so as to maintain the accuracy and stability. In the bubble interior stage, it is necessary to judge whether bubble nucleation occurs or not. If the bubble nucleation occurs, R_0, $\dot{n}$ and Λ_G are calculated by the heterogeneous nucleation theory of bubbles [9].

$$R_0=2\sigma/(P_{sat}-P_L) \quad (9)$$

$$\dot{n}=n_0\sqrt{\frac{3\sigma}{\pi m_0}}\exp\left(-\frac{16\pi\sigma^3}{3}\frac{\phi}{\lambda_L T_L}\frac{1}{(P_{sat}-P_L)^2}\right) \quad (10)$$

$$\Lambda_G=4\pi R_0^3\rho_G\dot{n}/3 \quad (11)$$

Here, Λ_G takes a value in the smallest class of the mass only. Each physical property is function of temperature and pressure. The pressure is calculated by using the balance between the liquid density and the volume fraction of liquid.

Results

Analysis on bubble growth and collapse in stationary liquid

Firstly, bubble nucleation and growth in a superheated liquid, and bubble collapse in a sub-cooled liquid were simulated. Figure 3(a) and (b) show void fraction, α_{Gi} 1/Kg, of each class, i, and the temporal change of bubble number-density, n_i 1/m^{3}Kg. As shown in Fig. 3 (a), number-density is increased due to the nucleation in the smallest class, i=1, the new bubble grows with time, and the bubble shifts to larger class, i>1. On the other hand, in the case of bubble collapse in a sub-cooled liquid as shown in Fig. 3(b), the existing bubble is contracted, it shifts to smaller class, and it finally becomes extinct at the smallest one. Figures 3(c) and (d) show the comparison of results by using the bubble size distribution model with various Δw. The Δw is the grid interval with respect to w. In addition results of single bubble growth and collapse without using bubble size distribution model (non-distribution model) are plotted. Almost the same results are obtained for various Δw. At $\Delta w=10^{-12}$, all bubbles are classified in the smallest class, therefore $\Delta w=10^{-13}$ is adopted. They can be calculated within the 5% error as compared to the non-distribution model.

Analysis on cavitating flow around NACA0015

Figure 4 shows the flow field. Grids have 84x21 or 172x50points to calculate a cavitating flow around NACA0015 foil. C-type grids are employed. Boundary condition is shown in table 1. Liquid nitrogen and liquid oxygen are employed as working fluids. Cavitation number, $\sigma=(P-P_{sat})/(0.5\rho_{in}V_{in}^2)$, is fixed at 0.15, inlet velocities are changed at 5, 10, 20 and 50m/s. Inlet temperatures are 90K in case of liquid nitrogen, and 90K and 110K in case of liquid oxygen. Angle of attack, AOA, is set at 4 and 8 degree.

Figure 5 shows spatial change of pressure coefficient, $-C_p=(P-P_{in})/(0.5\rho_{in}V_{in}^2)$, Mach number, M_a, and temperature difference, $\Delta T=(T-T_{in})$, from inlet temperature on the surface of the foil. All of cases have the same conditions, σ=0.15 and $|V_{in}|$=10m/s. At AOA=4 degree, cavitation hardly occurs. Therefore, $-C_p$, M_a and ΔT profiles are almost the same in all cases. At AOA=8 degree, however, partial cavitation occurs on the upper surface in case of LN_2 at 90K and LOX at 110K, and very small cavitation occurs near the leading edge on the upper surface in case of LOX at 90K. $-C_p$, M_a and ΔT profiles in cavitation region are different from that in non-cavitation region like LOX at 90K. In cavitation region, evaporation occurs and pressure approaches to

saturated pressure. Therefore, pressure coefficients, $-C_p$, in cases of LN_2 at 90K and LOX at 110K become smaller than that in case of LOX at 90K under non-cavitation. In addition, as cavitation region reduce the sound velocity due to the nature of two-phase fluid, Mach numbers, M_a, in cases of LN_2 at 90K and LOX at 110K are larger than that in case of LOX at 90K. The figure of ΔT indicates that nucleation occurs near x=0.05, cavitating bubbles grow from x=0.05 to x=0.3, and they collapse downward of x=0.3 in cases of LN_2 at 90K and LOX at 110K, because growth process brings temperature depression and collapse process brings temperature rising due to latent heat.

Figure 6 shows an effect of inlet velocity in case of LN_2, T_{in}=90K, σ=0.15 and AOA=8degree. In case of $|V_{in}|$=5m/s, cavitation does not happen. In all cases except $|V_{in}|$=5m/s, nucleation point is nearly the same position around the leading edge on the upper surface as shown in Fig. 6(a). Both Figures 6(a) and (b) show the cavitating region is formed by cavitation bubbles which are generated around the leading edge and grow as they move downward. Temperature depression and recover occur in cavitation region due to latent heat as shown in Fig. 6(c).

Figure 7 is enlarged figure of void fraction in case of $|V_{in}|$=10m/s, σ=0.15 and AOA=8degree. In all cases, nucleation point is nearly the same. Cavitation region in case of LN_2, however, is quite different from that in case of LOX at the same T_{in}=90K and the same σ=0.15. On the other hand, cavitation shape in case of LN_2 at 90K is similar to that in case of LOX at 110 K despite the different T_{in}. From the viewpoint of relative temperature to the critical one $T_r=T/T_c$, 110K of oxygen is corresponding to the 90K of nitrogen. But, maximum void fraction is not the same. This difference might be caused by a difference of physical property between LN_2 and LOX.

According to the above mentioned, LN_2 at 90K and LOX at 110K indicate a similar tendency qualitatively because of the same relative temperature T_r=0.71.

Analysis on cavitating flow around inducer

The LE-7A hydrogen turbo-pump inducer has 3 spiral foils. However, for simplicity, 2D calculation was carried out in unrolled channel at 0.9R cross-section from the center of its revolutions. Figure 8 shows the channel profile. Grids have 250x12points to calculate a cavitating flow around the inducer. The grids points move against the fluid at a peripheral velocity corresponding to the inducer revolutions. Boundary condition is shown in table 2. Liquid hydrogen is employed as working fluids.

Total inlet pressure, Pt_{in} is set at 100KPa, because cavitation is not generated at design point, Pt_{in}=260KPa. Pressure becomes minimum around the leading edge on the suction side of the foil. The foil increases pressure because it moves against the fluid on its pressure side. Therefore, pressure rises through the channel between the foils. Pressure becomes the maximum around the trailing edge on the pressure side of the foil.

Mach number increases between the foils. But it decreases to the former level.

Void fraction becomes the maximum around the leading edge on the suction side of the foil. This point is consistent with the minimum point of the pressure. However, because pressure is rapidly recovers, void fraction quickly decreases between the foils. Thereafter, pure liquid flow is achieved.

Maximum bubble radius increases with approach of the foil. It becomes the maximum around the leading edge on the suction side of the foil. This point is consistent with the minimum point of the pressure. This fact shows the inducer can collapse the cavitating bubbles.

The bubbles occur upstream of the foils and collapse between them. Cavitating flow in the inducer was successfully predicted by using the bubble size distribution.

Conclusion

A numerical code of cavitating flow with bubble size distribution model based on the bubble-mass has been developed. The present method was applied to cavitating flow around NACA0015 and a hydrogen turbo-pump inducer, and a reasonable behavior of bubble distribution was obtained which indicates the potential of the present method for the simulation of complex cavitating flows.

References

1) Ito, Y. & Nagashima, T.: Numerical simulation of sub-cooled LN_2 nozzle flow with cavitation, 2000, 5th International Symposium on Aero-thermodynamics of Internal Flows, pp. 715-722
2) Simoneau, R. J. & Hendricks, R. C.: Two-phase choked flow of cryogenic fluids in converging-diverging nozzles, 1979, NASA TP 1484
3) Tani, N., Nagashima, T.: Numerical analysis of cryogenic cavitating flow on hydrofoil - comparison between water and cryogenic fluids-, 2002, 4th Intl. Conference on Launcher Tech. "Space Launcher Liquid Propulsion"
4) Yuan, W., Sauer, J. & Schnerr, G. H.: Modeling and computation of unsteady cavitating flows in injection nozzle, 2001, Mec. Ind. 2, pp.383-394
5) Hao, Y. and Prosperetti, A.: The dynamics of vapor bubbles in acoustic pressure fields, 1999, Physics of Fluid, Vol.11 No.8, pp. 2008-2019
6) Ito, Y. Wakamatsu, H. & Nagasaki, T.: Numerical simulation of sub-cooled cavitating flow by using bubble size distribution, 2003, 6th International Symposium on Aerothermo-dynamics of Internal Flows, pp. 280-286
7) Shima, E. & Jonouchi, T.: Role of CFD in aeronautical engineering (No.12) AUSM type upwind schemes, 1994, 12th NAL Symposium on

Aircraft Computational Aerodynamics, pp. 255-260

8) Bram van Lee: Towards the ultimate conservative difference scheme, V. A. second-order sequel to Godunov's method, 1978, Journal of computational physics, 32, pp. 101-136

9) Van P. Carey: Liquid-vapor phase-change phenomena, 1992, Taylor & Francis

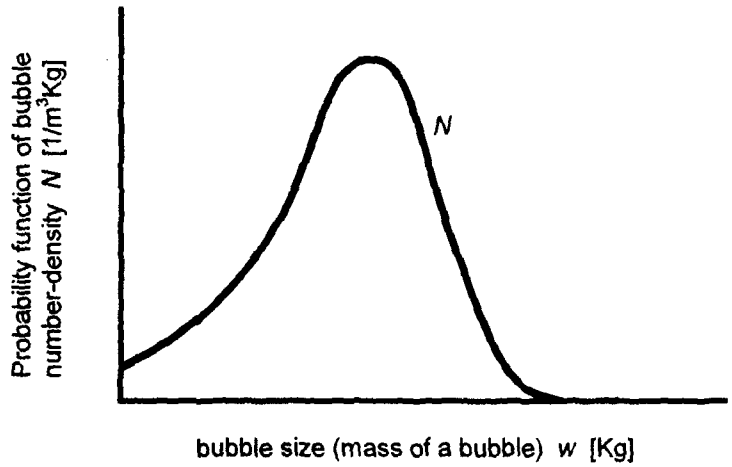

Fig. 1 Probability function of bubble number-density, N

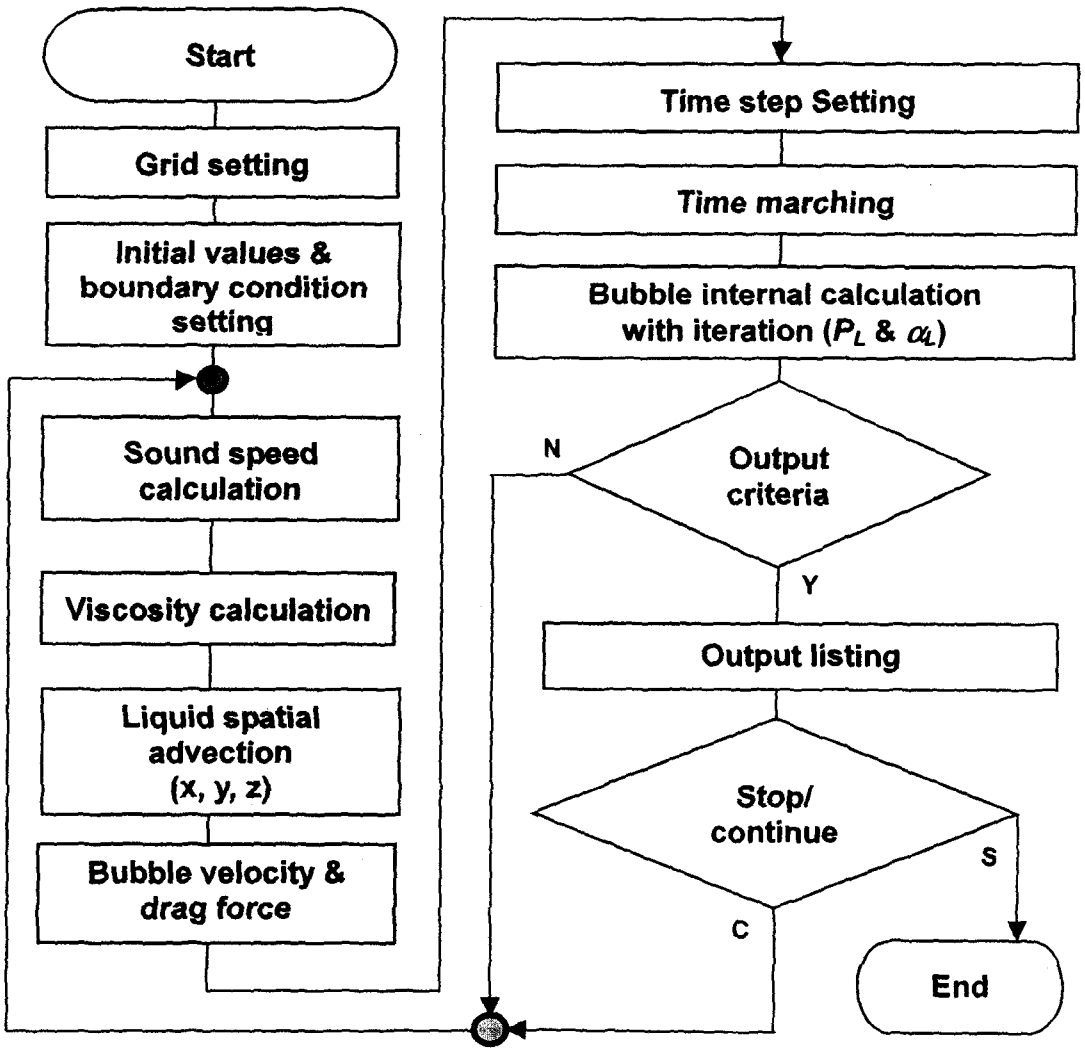

Fig. 2 Flowchart on calculation procedure

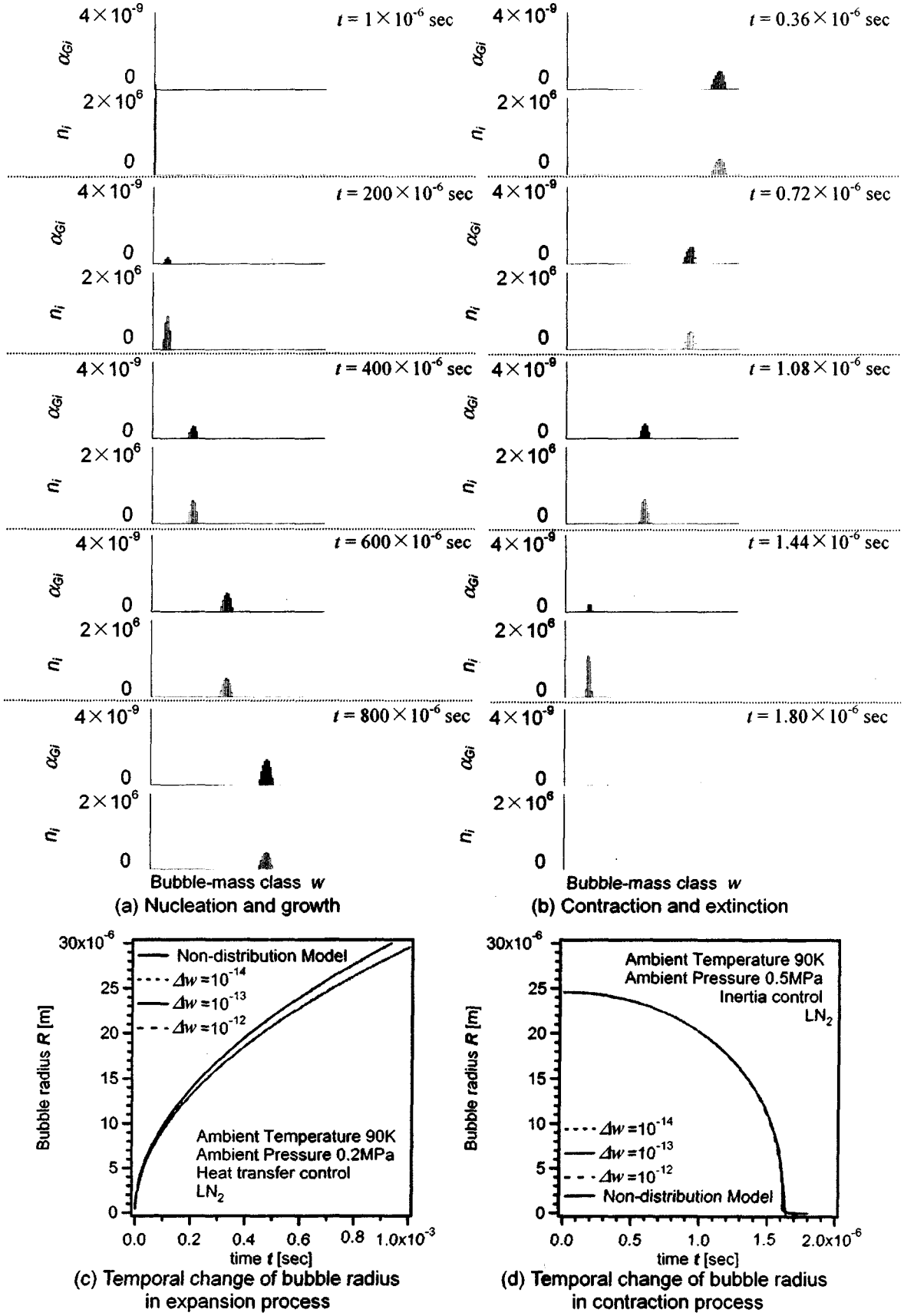

Fig. 3. Calculation by using the bubble size distribution model

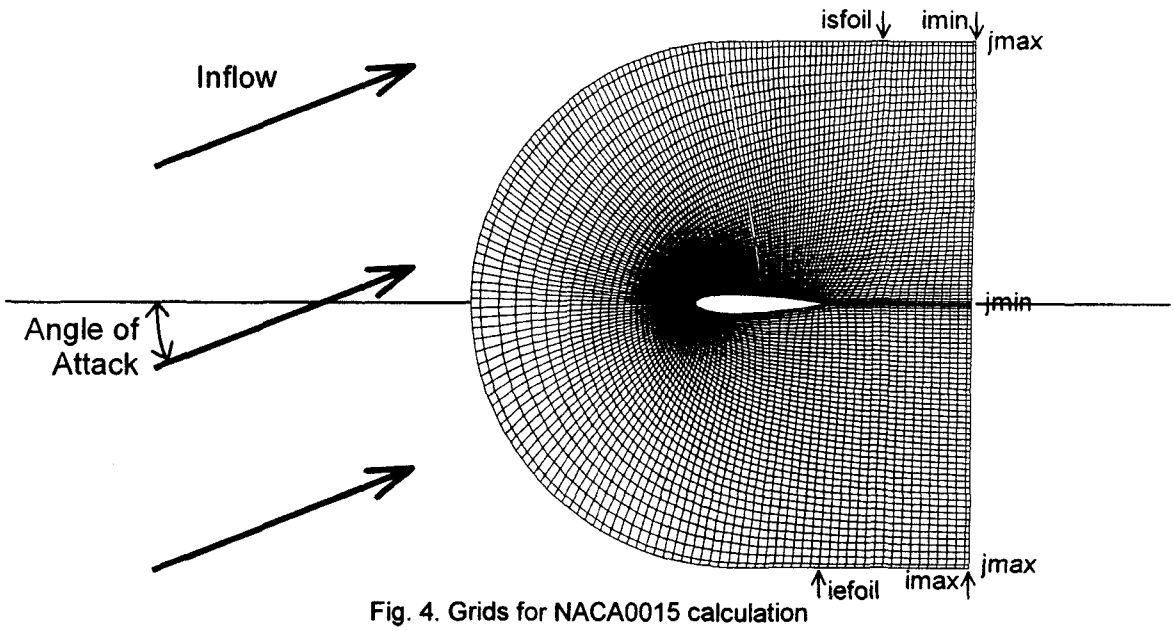

Fig. 4. Grids for NACA0015 calculation

Table 1. Boundary condition for NACA0015 calculation

Condition	Position	Pressure	Temperature	Velocity
Inlet & Outlet	i=imin ~ imax j=jmax	(inlet flow) •Constant (super-sonic outlet flow) •0 order extrapolation (sub-sonic outlet flow) •Constant	(inlet flow) •Constant (outlet flow) •0 order extrapolation	(inlet flow) •Constant (outlet flow) •0 order extrapolation
Outlet	i=imin & imax j= jmin ~ jmax	(super-sonic outlet flow) •0 order extrapolation (sub-sonic outlet flow) •Constant	•0 order extrapolation	•0 order extrapolation
Periodic	i=imin ~ isfoil & i=iefoil ~ imax j=jmin	•Copy from the corresponding point	•Copy from the corresponding point	•Copy from the corresponding point
Foil surface	i= isfoil+1 ~ iefoil-1 j=jmin	•0 order extrapolation	•0 order extrapolation	•Stationary

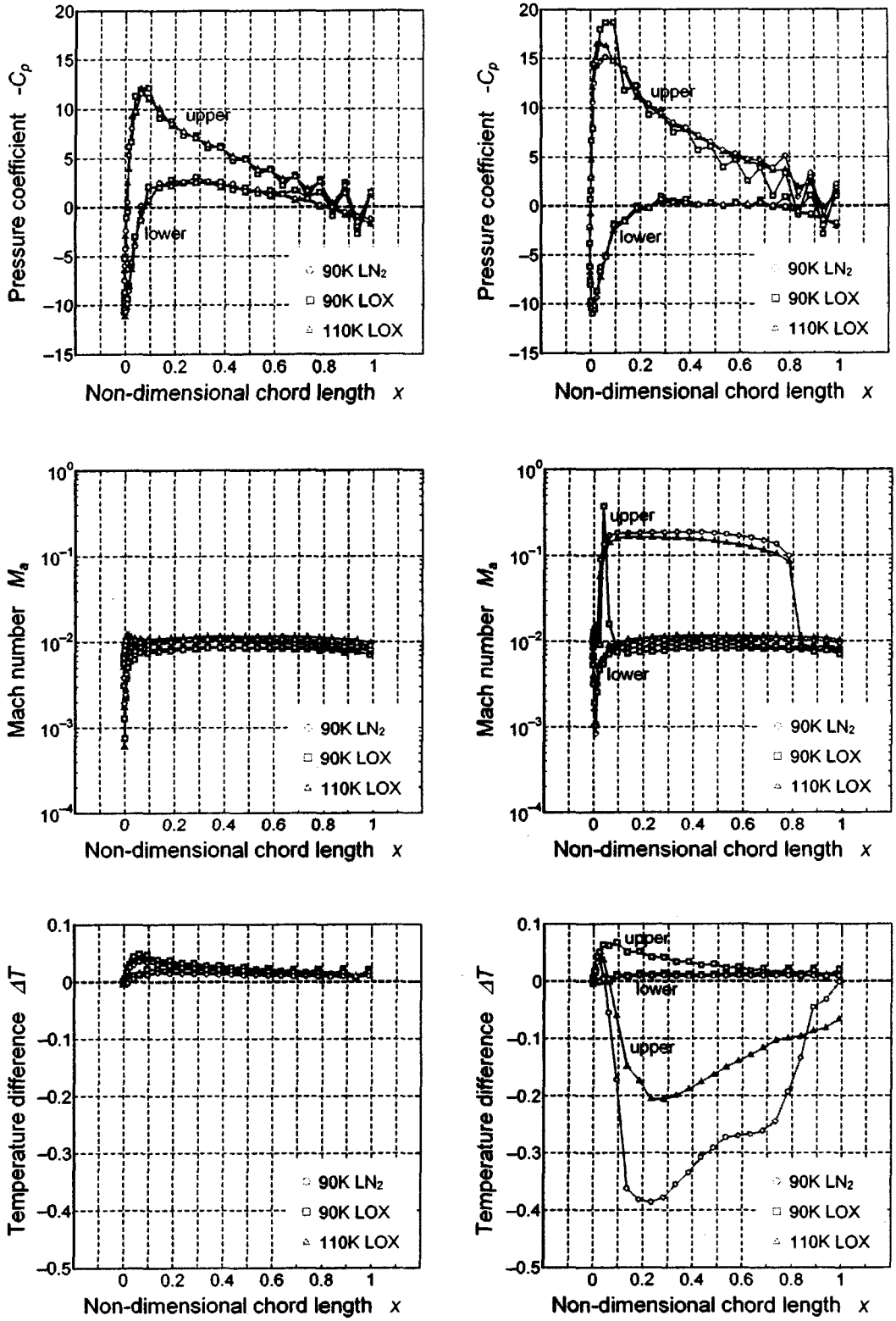

(a) *AOA* = 4deg

(b) *AOA* = 8deg

Fig. 5. Pressure coefficient, -*Cp*, and Mach number, *Ma*, and temperature difference, ΔT on NACA0015 (σ=0.15, $|V_{in}|$=10m/s)

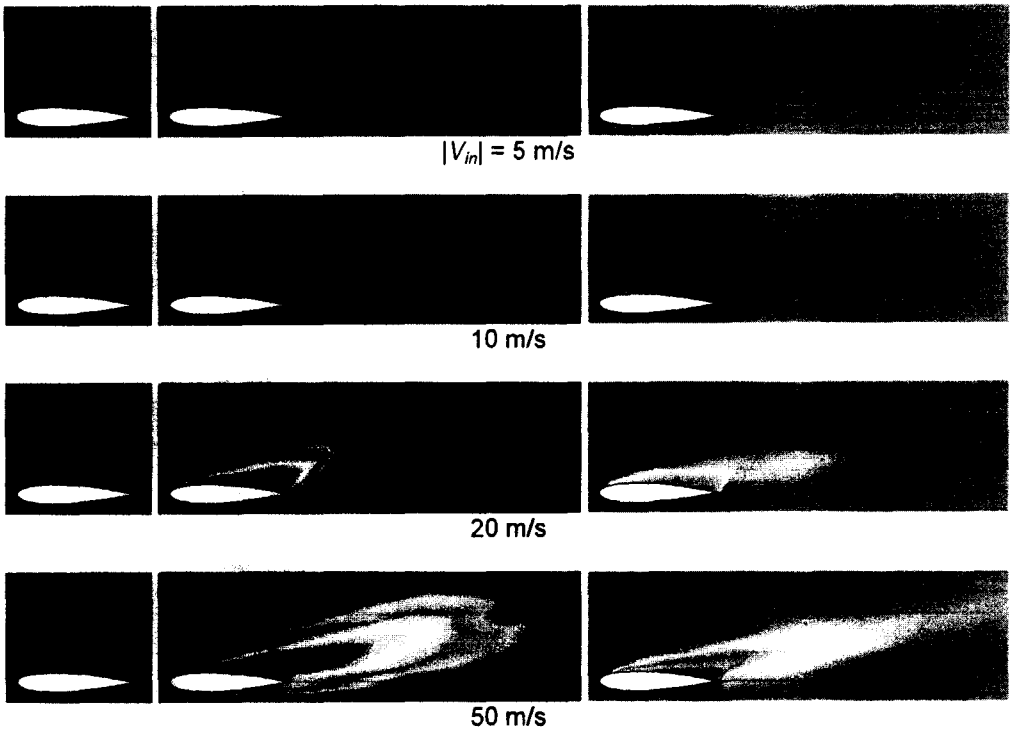

Fig. 6. Effect of inlet velocity: V_{in} (LN_2, T_{in} = 90K, σ= 0.15, AOA =8deg)

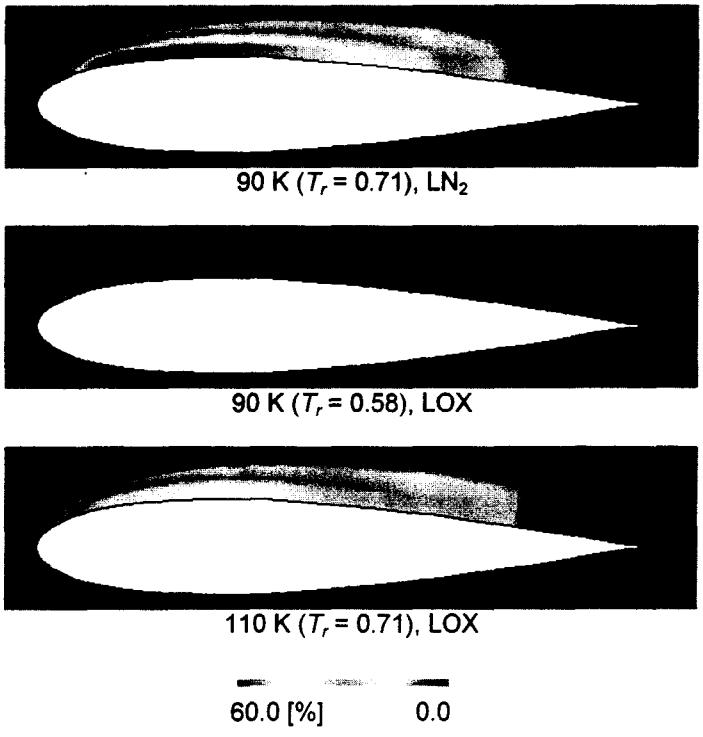

Fig. 7. Void fraction profiles ($|V_{in}|$ = 10m/s, σ= 0.15, AOA = 8deg)

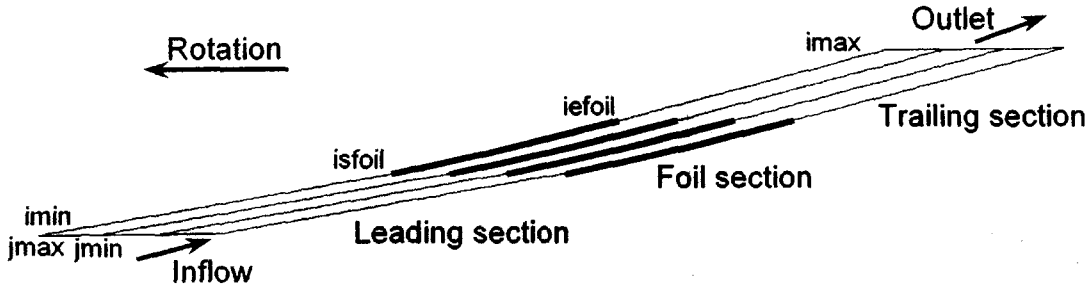

Fig. 8. Channel profile of 3 channels at 0.9R cross-section of the LE-7A hydrogen inducer (2D calculation)

Table 2. Boundary condition for the LE-7A hydrogen inducer

Condition	Position	Pressure	Temperature	Velocity
Inlet	i=imin j= jmin ~ jmax	•Total pressure Constant	•Constant	•0 order extrapolation
Outlet	i=imax j= jmin ~ jmax	(super-sonic outlet flow) •0 order extrapolation (sub-sonic outlet flow) •Constant	•0 order extrapolation	•0 order extrapolation
Periodic	i=imin ~ isfoil & i=iefoil ~ imax j=jmin & jmax	•Copy from the corresponding point	•Copy from the corresponding point	•Copy from the corresponding point
Foil surface	i= isfoil+1 ~ iefoil-1 j=jmin & jmax	•0 order extrapolation	•0 order extrapolation	•Stationary

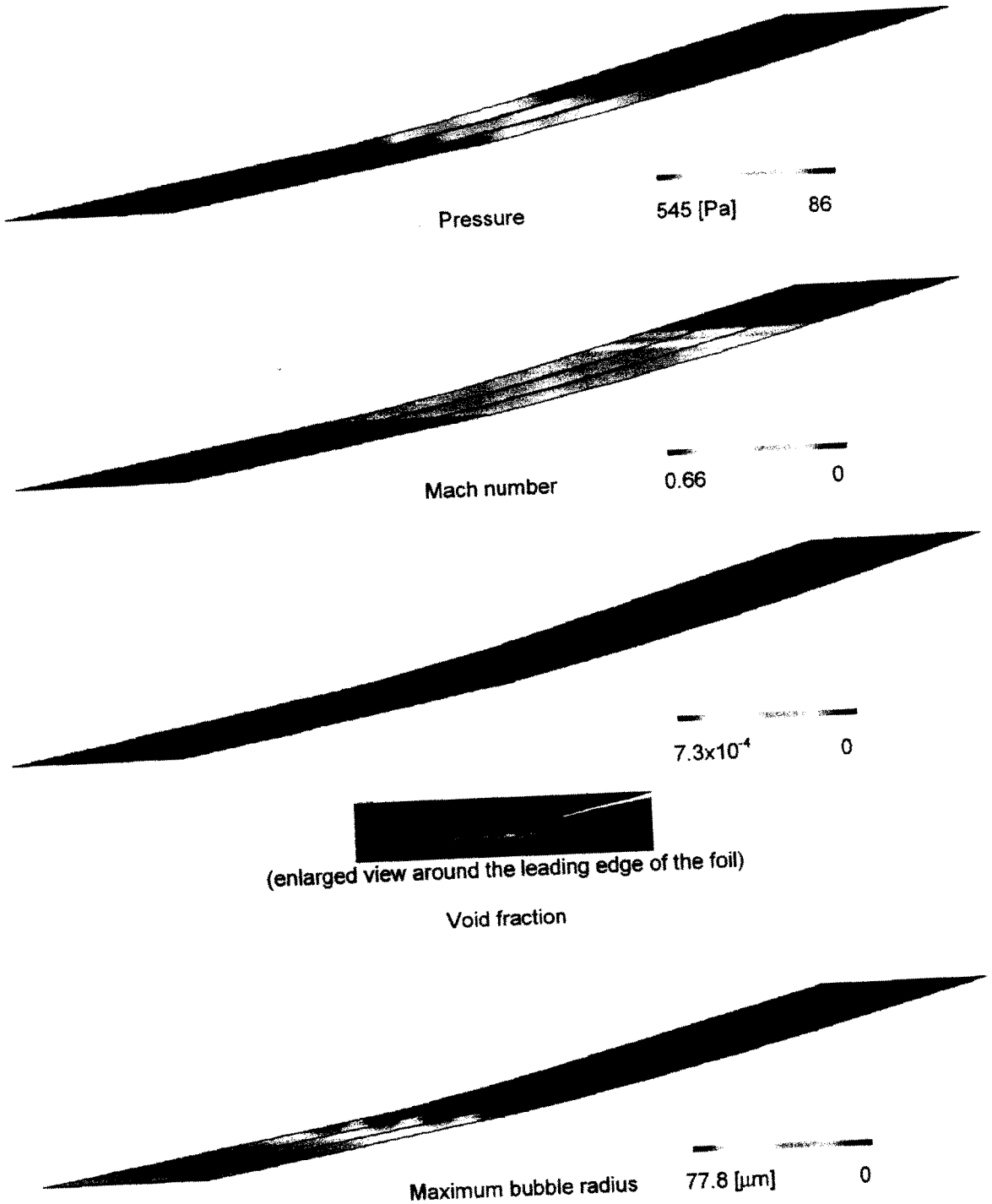

Fig. 9. Results for the LE-7A hydrogen inducer
(LH_2, ϕ=163.8mm, 46100rpm, T_{in}=21K, Pt_{in}=100kPa, P_{out}=520kPa)